Kinematic mixing and heat transfer enhancement in chaotic split-and-recombine heat exchangers/reactors

Akram Ghanem, Thierry Lemenand, Dominique Della Valle, Hassan Peerhossaini

HAL Id: hal-03287160

https://univ-angers.hal.science/hal-03287160

Submitted on 15 Jul 2021

Kinematic Mixing and Heat Transfer Enhancement in Chaotic Split-And-Recombine Heat Exchangers/Reactors

Akram Ghanem[1,a], Thierry Lemenand[1,b], Dominique Della Valle[1,2,c] and Hassan Peerhossaini[3,d]

[1] LUNAM Université, Laboratoire de Thermocinétique Nantes, CNRS UMR 6607, Nantes, France

[2] ONIRIS, Nantes, France

[3] Univ. Paris Diderot, Sorbonne Paris Cité, Institut des Energies de Demain (IED), Paris, France

[a] akram.ghanem@univ-nantes.fr, [b] thierry.lemenand@univ-nantes.fr,
[c] dominique.dellavalle@oniris-nantes.fr, [d] hassan.peerhossaini@univ-paris-diderot.fr

Abstract. Small system dimensions, low fluid velocity and high viscosity are all factors that hinder the production of turbulence. Enhancing mixing and heat transfer under these conditions, while keeping sufficient residence times and moderate pressure drops, constitutes a real challenge. Adapted to low-Reynolds flow regimes, Split-And-Recombine (SAR) static mixer and heat exchanger configurations are designed to exploit flow energy to produce chaotic advection and promote diffusion at the molecular level. The present work explores the hydrodynamic and thermal character of the SAR flow and compares, through CFD simulations, two such geometries namely SAR-1 and SAR-2, with two other reference configurations: a square three-dimensional continuous flow geometry (3D-Flow) and a plain square channel. Efficient convective heat transfer is achieved in deeply laminar creeping flow. Relative enhancements up to 1700% can be achieved compared to plain square channel flow, with a moderate increase in the pressure drop that does not exceed 17% for the SAR-2 configuration showing the better performance.

Introduction

Multifunctional heat exchangers/reactors are containers for thermally active chemical synthesis processes with high safety and efficiency requirements demanding good flow mixing properties and often manipulating fragile fluid structures. In addition, a primary challenge in this type of technology is to increase the heat removal, or supply, in the system while working in the laminar regime to maintain sufficient residence time for reactive chemistry, or in the case turbulence is hindered by the microsystem dimensions. Mixing, heat transfer, and dispersion can be difficult because of the large energy costs of processing these fluids due to their shear-sensitive complex-structure rheology and possible irreversible denaturation [1,2].

One of the ways to intensify transport phenomena is then to create particular three-dimensional chaotic structures in the steady flow reaction path [3,4,5], as in the chaotic flux recombination reactors discussed here and shown in Fig. 1 (a) and (b). The configuration names SAR-1 and SAR-2 reflect the number of splits and recombinations in the repetitive elementary unit. They were first proposed on a microscale by Gray et al. [6] and Chen and Meiners [7] respectively. The network of separated and then recombined channels in these configurations creates chaotic structures while maintaining the flow in the laminar regime. They present topological structures that exploit the flow laminarity to fold the flow repeatedly and double the lateral concentration gradient deterministically, thus obtaining fast and efficient mixing by diffusion in a very compact geometry. This topology performs a series of baker's transforms [8] on the fluid layers and consequently on eventual tracer concentration profiles.
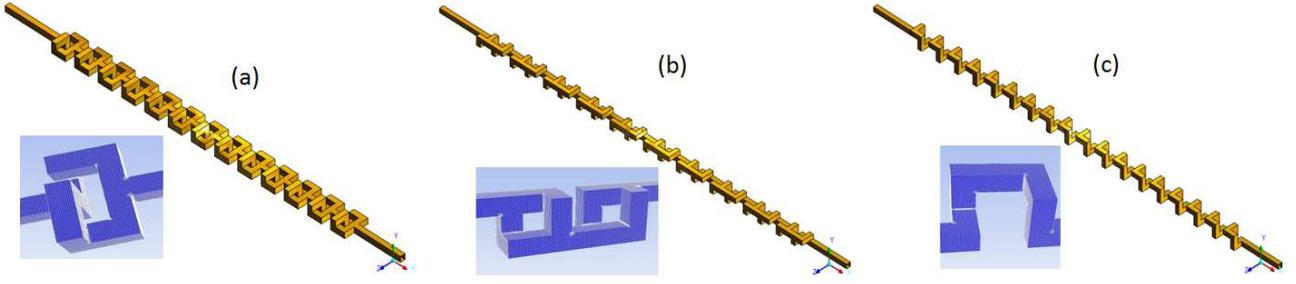
Fig. 1. Elementary units and global 3D views of the studied configurations: (a) SAR-1, (b) SAR-2, and (c) 3D-Flow.

The two fluid streams are combined, split out of the plane, rotated, and recombined, folding the concentration profile and doubling the lateral striation. Successive separation and reuniting of fluid streams increases the number of laminates, so that the contact area between the two fluids is increased at a theoretical rate of 2^n, with n the number of iterations, resulting in faster mixing by diffusion and enhanced heat transfer without generating prohibitive losses [9].

Modeling and Numerical Simulation

The solver used for the laminar, steady, three-dimensional flow computations is the CFD code FLUENT®. The computational mesh is a cell-centered finite volume discretization. The solver is a double-precision, segregated, steady, implicit linearization finite volume solver. Pressure-velocity coupling is achieved by the Semi-Implicit Method for Pressure Linked Equations-Consistent (SIMPLEC) algorithm [10]. Spatial discretization schemes are second order upwind for momentum and energy, and PRESTO staggered variable arrangement for pressure to ensure a maximum accuracy for the cell face pressure calculation in the strongly curved domains.

The hydraulic diameter of all the channels considered here is D_h=3 mm, and the developed length L=750 mm (sum of the constituting elementary channels on the central line). A fixed dynamic viscosity of 10 Pa.s is used for the flow simulations. The other fluid physical properties are the same as those of water at 300 K. In the entrance region, a uniform fluid velocity U is introduced, while a pressure outlet condition is applied at the exit. The inlet velocity is varied between 3.3×10^{-4} and 33 m s^{-1} for a corresponding flow rate between 3×10^{-6} and 0.3 kg s^{-1}. Reynolds number thus varies between 10^{-4} and 10. The fluid enters the inlet with a temperature of 300 K and is assumed to preserve constant physical properties throughout the test section. It is heated by a thermal flux at the wall that is maintained at a constant temperature of 360 K. Impermeable boundary and no-slip wall conditions are implemented over the duct walls. The zero value of the pressure at the outlet is a reference point for the pressure gradient integration. The parameters of interest in the present study are the Reynolds number Re, the Péclet number Pe, the local heat flux density φ_x, the wall and bulk temperatures (T_w and T_b respectively), the convective heat transfer coefficient h, the Nusselt number Nu, the pressure drop ΔP, the major head loss coefficient λ, and the thermal enhancement factor η_t. Calculations are based on the constant fluid properties: density ρ, dynamic viscosity μ, thermal conductivity κ, and thermal diffusivity α. Table 1 resumes the different parameters and their respective expressions. The subscript 'x' represents local values and the subscript '0' represents quantities corresponding to a plain square channel flow.

Table 1. Significant parameters and their calculation methods.

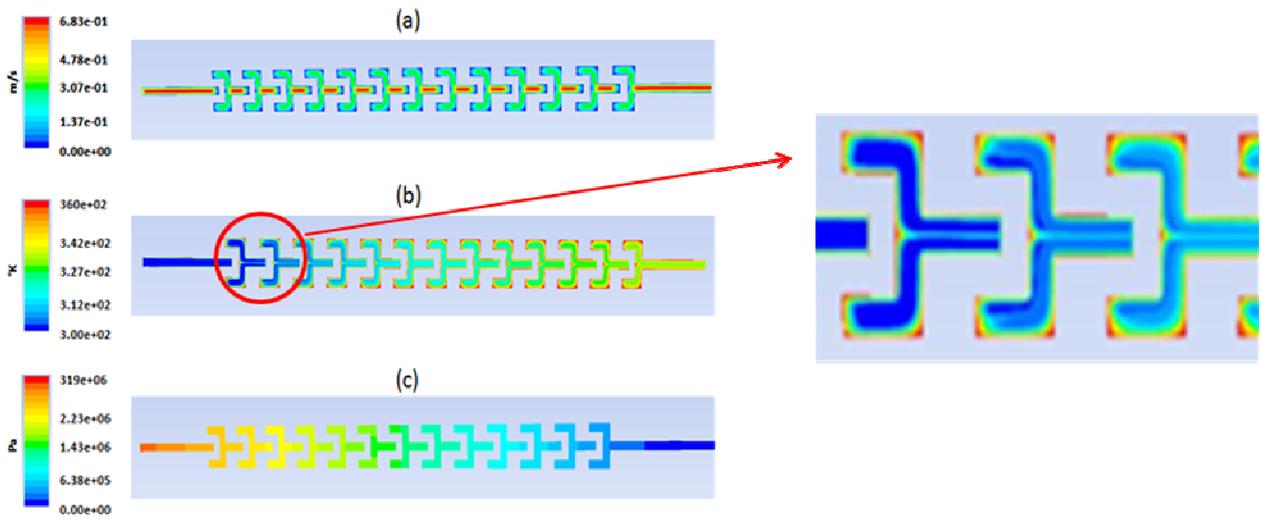|			
$Re = \dfrac{\rho U D_h}{\mu}$	$Pe = \dfrac{U D_h}{\alpha}$	$h_x = \dfrac{\varphi_x}{(T_w - T_b)_x}$	$Nu_x = \dfrac{h_x D_h}{\kappa}$
$Nu = \dfrac{1}{A}\int Nu_x \partial A$	$\lambda = \dfrac{(\Delta P / L)D_h}{\frac{1}{2}\rho U^2}$	$\eta_t = \left(Nu \big/ Nu_0\right)\Big/\left(\lambda \big/ \lambda_0\right)^{1/3}$	

Fig. 2. Contours of (a) velocity, (b) temperature (with a blow-up of the encircled area), and (c) pressure for *Pe*=7000 and *Re*=0.1 in the median plane of SAR-1.

To determine the appropriate density of the mesh, we conducted a series of simulations in one of the geometries (SAR-1), considering 13 repetitive elements. Starting with a coarse initial mesh, it is gradually refined till the produced results remain unchanged. The lowest density mesh giving satisfactory results was adopted as a compromise between precision and calculation time. The chosen mesh is used in both of the studied SAR configuration, the 3D-Flow configuration, and the plain channel.

Velocity field. After the inlet length of 10 diameters, a parabolic velocity profile is established in the cross-section and is slightly disturbed by the flow curvature. Dealing with the entire set of pathlines, it is evident that little transverse activity is produced and the fluid seems to follow the channel walls in a parallel motion and the only significant variation, shown in Fig. 2 (a) is the doubling of the velocity magnitude as the split streams are recombined, creating higher flow inertia in the sections connecting two consecutive SAR units. Low-velocity stagnation zones prevail around the corners of the concave outer walls of the bent configurations. On the contrary, the convex corners contribute to the rupture of the hydrodynamic boundary layer on the adjacent walls and the local axial velocity magnitude is consequently higher yet with no significant deformation of the fluid trajectories and the velocity vectors. Following the same reasoning, for the same inlet Reynolds number, higher global velocities prevail in the 3D-Flow configuration where no splitting takes place.

Convective heat transfer. Mass and heat transfer are two closely related phenomena since heat energy transmitted through the wall by pure conduction is the transported by fluid particles through convection and diffusion. A close inspection of Fig. 2 (a) and 2 (b) reveals the link between the velocity and the temperature fields, in addition to the imprints of the SAR mechanism on the heat transfer map in the chaotic exchanger. The low-velocity zones around the concave corners of the bends exhibit poor heat evacuation from the wall region to the core flow and local overheated fluid zones are produced, where convective heat transfer is weak. A close look at the temperature contours in the linear section between the first two elements shows the existence of a hot strip in the flow core between two colder zones from above and below. In conventional heat transfer devices, the core flow is the coldest region, being the farthest from the walls. Here, the hot zone is the signature of the SAR mechanism.
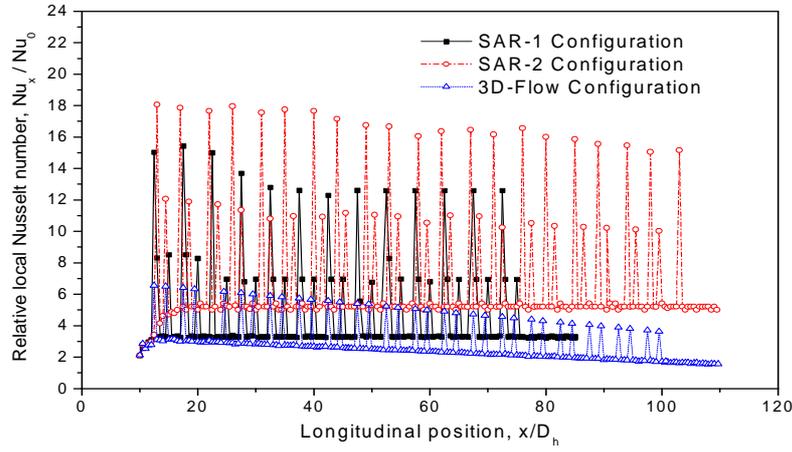
Fig. 3. Longitudinal variation of the relative local Nusselt number.

It should also be noted that in the direct vicinity of the diverging zone where fluid streams are split, a sharp increase in the surface heat flux is recorded in both SAR configurations: the local Nusselt numbers downstream from the splitting zones exhibit sharp peaks visible in Fig. 3, which plots the local Nusselt numbers in the bent configurations normalized by their corresponding values in the plain square channel, Nu_0. These high amplitude peaks are naturally absent in the 3D-Flow configuration where no splitting occurs. Albeit, this configuration exhibits smaller amplitude peaks: the signature of the boundary layer destruction and possible instabilities at the convex corners of the sharp bends. This phenomenon is also seen in the two other configurations that also exhibit abrupt modifications of the flow direction and is conveyed by the shorter apices of the plot in Fig. 3.

The variation of the relative global Nusselt numbers with Re is plotted in Fig. 4, where Nu increases with Re as the rate of advection increases in the flow for the same level of diffusion. Examining the tendencies of the slopes in the different zones of Fig. 4, it can be seen that for the three configurations, the relative enhancement with respect to a plain channel rapidly increases with Re in the intermediate region of studied Reynolds numbers *i.e.* between 0.01 and 1 beyond which the relative increase diminishes. Heat transfer in the SAR-2 configuration is favored by its high ratio of number of splits/recombinations to the total developed length, together with the higher average velocity compared to SAR-1. In order to better compare the global performance, we present in the following section an analysis of the produced head losses and overall thermal enhancement.

Performance evaluation. The major head loss coefficients are calculated from the total pressure drop using the volume-averaged fluid velocity in each configuration.

Fig. 5 displays the variation of the normalized major head loss coefficient, $\lambda/\lambda0$ with the inlet Reynolds number whose values range between 10^{-4} and 10. Major losses in the SAR-2 configuration exceed those in SAR-1 due to higher average velocities. SAR-1 incorporates more bends per unit but in SAR-2 the fluid undergoes a larger number of splits and recombinations. In fact, for this range of low Reynolds numbers, the contribution of singularities (splits, recombinations, and bends) to the pressure drop appears to be negligible. The ratio tends to increase with the rise of Re values as the flow velocity increases and energy consumption becomes more important. Major losses in the SAR-2 configuration exceed those in SAR-1 due to higher average velocities. SAR-1 incorporates more bends per unit but in SAR-2 the fluid undergoes a larger number of splits and recombinations. In fact, for this range of low Reynolds numbers, the major head loss coefficient exceeds by far the minor coefficient of all singularities, and minor losses become negligible. For low Re, 3D-Flow consumes the least energy yet its consumption increases at a higher rate than the SAR configurations similarly owing to flow velocity considerations.
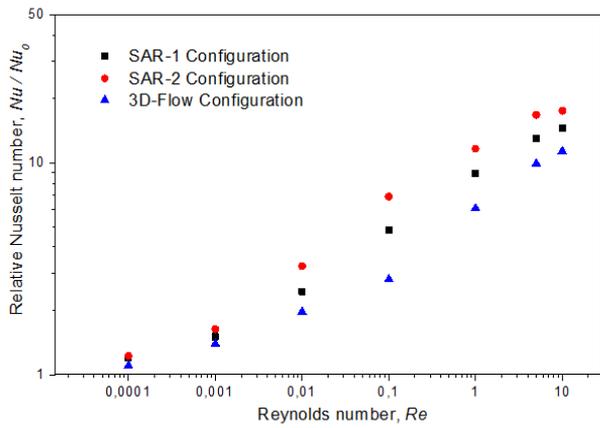
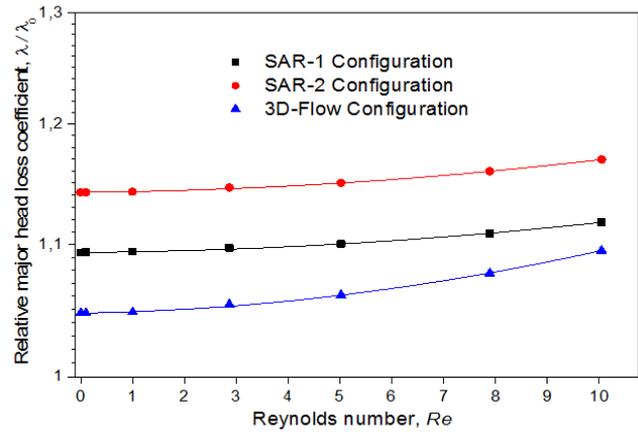Fig. 4. Relative Nusselt number versus Reynolds number.

Fig. 5. Relative major head loss coefficient versus Reynolds number.

More important than its evolution, is the magnitude of the relative major head loss coefficient. For the produced heat transfer enhancement, one expects that the chaotic configurations produce exponential increases in head losses, which is not the case. For example, around $Re=10$, compared to a plain channel, SAR-2 enhances Nusselt number by 18 folds with a mere 17% increase of the major head loss coefficient. The absence of flow blockage and the exploitation of the flow's own energy to enhance transport render the SAR configurations feasible for laminar flow applications where, expectedly, the global gain in the system energy balance exceeds that of other enhancement techniques as additional thermal power is transferred with moderate energy consumption.

In order to better characterize the link between the thermal gain and the accompanying energy expenditures, the thermal enhancement factor η_t introduced in Table 1 is calculated. Fig. 6 presents the variation of this factor in terms of Reynolds number. This term quantifies the ratio of the modified geometry surface heat transfer coefficient to that of a plain geometry at equal pumping power. As expected, η_t tends to increase with increasing Re. The three configurations show similar heat transfer qualities for $Re<10^{-2}$. More important on this plot is that, from an energy efficiency perspective, SAR-2 conserves the best position conveyed by the global Nu plot although it produces higher head losses. The relative enhancement in Nu is more significant than the accompanying increase in the major head loss coefficient. At its best, for $Re=5$, SAR-2 performs 28% better than SAR-1 and 65% better than 3D-Flow.
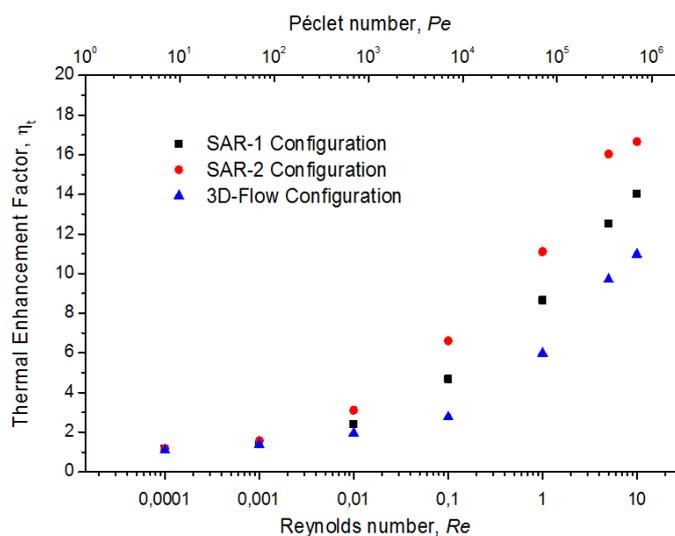

Fig. 6. Thermal enhancement factor versus Reynolds and Péclet numbers.

Conclusions

Chaotic laminar flow and convective heat transfer in a three-dimensional continuous flow and two Split-And-Recombine multifunctional heat exchangers/reactors are numerically investigated. Surface curvature and periodic flow deviations create spatial chaos within the configurations. The SAR mechanism promotes chaos by exponentially increasing the interfacial area between the different fluid layers created by the consecutive diverging and converging zones of the geometries. Dynamic particle trajectories and periodic variations in the local velocity field enhance mass transport. Heat transmitted to the fluid molecules through the constant temperature walls is readily diffused throughout the entire section and high convective heat transfer rates contribute to the homogenization of the cross sectional temperature. Structural singularities produce even higher transfer rates reflected through localized abrupt increases in the surface Nusselt number. Efficient heat transfer is achieved in deeply laminar creeping flow. Relative enhancements up to 1700% can be achieved compared to plain square channel flow, with a moderate increase in the pressure drop that does not exceed 17% in the worst studied case. The SAR-2 configuration exhibits the best performance: 28% better than the SAR-1 and 65% better than 3D-Flow. Increased splitting/recombination steps and a better optimization of the velocity field distribution account for the higher efficiency. The chaotic configurations perform best for the intermediate values of Re between 0.01 and 1 where the flow energy is most efficiently exploited to enhance mixing and heat transfer.

Upscaled from the microfluidic laboratory domain, the geometric characteristics of the optimized configurations permit them to handle flow rates characteristic of modern process industry. This type of reactor can be widely used in pharmaceutical, cosmetic, chemical and food industries where handling viscous, fragile and sometimes reactive flows are a real challenge.

References

[1] D Lester, D. R., Rudman, M., Metcalfe, G., 2009, "Low Reynolds number scalar transport enhancement in viscous and non-Newtonian fluids," Int. J. Heat Mass Trans. (52), pp. 655-664.

[2] Metcalfe, G., Lester, D., 2009, "Mixing and heat transfer of highly viscous food products with a continuous chaotic duct flow," J. Food Eng., 95, pp. 21–29.

[3] Ottino, J.M., 1989, "The Kinematics of Mixing: Stretching, Chaos and Transport," Cambridge University Press, New York.

[4] Wiggins, S., Ottino, J.M., 2004, "Foundations of chaotic mixing," Philos. Trans. R. Soc. London (A), 362, p. 937.

[5] Schönfeld, F., Hessel, V., Hofmann, C., 2004, "An optimised split-and-recombine micro-mixer with uniform 'chaotic' mixing," Lab Chip, 4, pp. 65–69.

[6] Gray, B. L., Jaeggi, D., Mourlas, N. J., Van Drieënhuizen, B. P., Williams, K. R., Maluf, N. I., Kovacs, G. T. A., 1999, "Novel interconnection technologies for integrated microfluidic systems," Sensors Actuators, 77, pp. 57-65.

[7] Chen, H., Meiners, J. C., 2004, "Topologic mixing on a microfluidic chip," Appl. Phys. Lett., 84(12), pp. 2193-2195.

[8] Carrière, P., 2007, "On a three-dimensional implementation of the baker's transformation," Physics of fluids, 19 (11), n°118110.

[9] Lester, D.R., Rudman, M., Metcalfe, G., 2009, "Low Reynolds number scalar transport enhancement in viscous and non-Newtonian fluids," Int. J. Heat Mass Trans., 52, pp. 655–664.

[10] Vandoormaal, J.P., Raithby, G.D., 1984, "Enhancements of the SIMPLE method for predicting incompressible fluid flows," Numer. Heat Tr., 7, pp. 147–163.